Asymmetric Josephson effect in inversion symmetry breaking topological materials

Chui-Zhen Chen,[1] James Jun He,[1] Mazhar N. Ali,[2] Gil-Ho Lee,[3,*] Kin Chung Fong,[4,†] and K. T. Law[1,‡]

[1]*Department of Physics, Hong Kong University of Science and Technology, Clear Water Bay, Hong Kong, China*

[2]*Max Plank Institute for Microstructure Physics, Weinberg 2, 06120 Halle, Germany*

[3]*Department of Physics, POSTECH, Pohang, South Korea*

[4]*Raytheon BBN Technologies, Quantum Information Processing Group, Cambridge, Massachusetts 02138, USA*

(Received 2 May 2018; revised manuscript received 25 June 2018; published 27 August 2018)

Topological materials which possess topologically protected surface states have attracted much attention in recent years. In this work, we study the critical current of superconductor/inversion symmetry breaking topological material/superconductor junctions. We found surprisingly that, in topological materials with broken inversion symmetry, the magnitude of the critical Josephson currents $|I_c^+(B)|$ at fixed magnetic field B is not the same for critical currents $|I_c^-(B)|$ flowing in the opposite direction. Moreover, the critical currents violate the $|I_c^\pm(B)| = |I_c^\pm(-B)|$ relation and give rise to asymmetric Fraunhofer patterns. We call this phenomenon asymmetric Josephson effect (AJE). AJE can be used to detect inversion symmetry breaking in topological materials such as in quantum spin Hall systems and Weyl semimetals.

DOI: 10.1103/PhysRevB.98.075430

I. INTRODUCTION

Over the past decade, there has been an intense interest in the study of topological materials such as topological insulators which possess surface states [1,2]. The surface states are protected by the bulk insulating gap and time-reversal symmetry. In more recent years, it was shown that protected surface states can exist even in gapless systems such as Weyl semimetals when inversion symmetry breaking splits a Dirac point into two Weyl points with opposite chirality [3–6]. The projections of the Weyl points on the surface Brillouin zones are connected by Fermi arcs which result in conducting surface states on the Weyl semimetal. Surface Fermi arcs have been observed experimentally through angle resolved photoemission spectroscopy (ARPES) experiments [7–10]. However, the transport studies of Weyl semimetals have been mostly focused on chiral anomaly [11–14] and other bulk properties of Weyl semimetals [15–19]. On the other hand, electronic transport signatures of Fermi arc states of Weyl semimetals have not been well explored theoretically and experimentally [20–23]. We shall investigate the direct transport signature of inversion symmetry breaking in these topological materials.

In this work, we study the critical currents I_c as a function of magnetic field B in a superconductor/inversion symmetry breaking topological material/superconductor Josephson junction as depicted in Fig. 1. The Josephson current of the junction is mediated by the edge states or surface states as well as the bulk states of the topological material. We show that the magnitude of critical current across the junction $|I_c^+(B)|$ does not equal the critical current flowing in the opposite direction $|I_c^-(B)|$ at fixed magnetic field B such that $|I_c^+(B)| \neq |I_c^-(B)|$. Moreover, the critical currents are different when the magnetic field switches sign, namely, $|I_c^\pm(B)| \neq |I_c^\pm(-B)|$. This gives rise to asymmetric Fraunhofer patterns. This phenomenon is in sharp contrast to conventional Josephson junctions in which $|I_c^\pm(B)| = |I_c^\pm(-B)|$ and I_c is independent of the direction of the Josephson current. We call this phenomenon asymmetric Josephson effect (AJE). Particularly, we show that AJE is particularly pronounced for the edge/surface states and it can be used to detect the inversion symmetry breaking effects in Weyl semimetal through the Fermi arc induced AJE.

To understand the origin of AJE in topological materials, we first start with a Josephson junction formed by two superconductors and an inversion symmetry breaking two-dimensional (2D) topological insulator with helical edge states. Due to inversion symmetry breaking, the top (blue) and bottom (red) helical edge states have different Fermi velocities as depicted in Fig. 2 [24]. In the Josephson junction, the superconductors induce a superconducting gap on the edge states and create Andreev bound states. Due to different Fermi velocities, the Andreev bound-state spectrums of the top and bottom edges are different as depicted in Fig. 3. This results in different Josephson current contributions from the top and bottom edges. Furthermore, the magnetic field generates a phase difference between the two Josephson current channels on the two edges and results in AJE. The AJE is manifested by the asymmetric Fraunhofer pattern of the Josephson junction as shown in Figs. 2(c) and 2(d). As shown in Fig. 4, we show that the Fermi arc states of Weyl semimetals can give rise to pronounced AJE.

II. AJE IN 2D TOPOLOGICAL INSULATOR WITH BROKEN INVERSION SYMMETRY

To start with, we study a superconductor/2D topological insulator/superconductor junction. The 2D topological insulator is described by a square lattice with four orbitals on each site

*lghman@postech.ac.kr
†kc.fong@raytheon.com
‡phlaw@ust.hk

 ©2018 American Physical Society

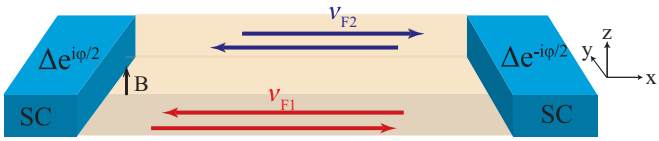

FIG. 1. Schematic picture of a superconductor/topological material/superconductor junction where φ is the phase difference between two superconductors. The edge (or surface) states on two sides of a topological material have different Fermi velocities v_{F1} and v_{F2} when inversion symmetry is broken and this can give rise to asymmetric Josephson effect (AJE) in the presence of magnetic field B.

[25] with an additional term which breaks inversion symmetry:

$$H_{TI} = \sum_{k_x,k_y} \psi^\dagger_{\mathbf{k}} \{\Gamma \sin k_x \tau_0\sigma_3 + M_{\mathbf{k}}\tau_3\sigma_0 + A \sin k_x \tau_1\sigma_3 + A \sin k_y \tau_2\sigma_0\}\psi_{\mathbf{k}}, \quad (1)$$

where the Pauli matrices $\tau_{1,2,3}$ (σ_3) and the unit matrix $\tau_0(\sigma_0)$ are defined in the orbital (spin) space, and $\psi^\dagger_{\mathbf{k}}$ is a four component fermionic operator. $M_{\mathbf{k}} = m_0 + 2m_1(2 - \cos k_x - \cos k_y)$ determines the energy gap of the system with the momentum $k_{x,y}$ and A couples two orbitals. When the Γ term is nonzero, the inversion symmetry is broken because $\mathcal{P}H_{TI}(-\mathbf{k})\mathcal{P}^{-1} \neq H_{TI}(\mathbf{k})$ with $\mathcal{P} = \tau_3\sigma_0$ [24].

Figures 2(a) and 2(b) depict the energy spectrums of the system in the topological regime with an open-boundary condition

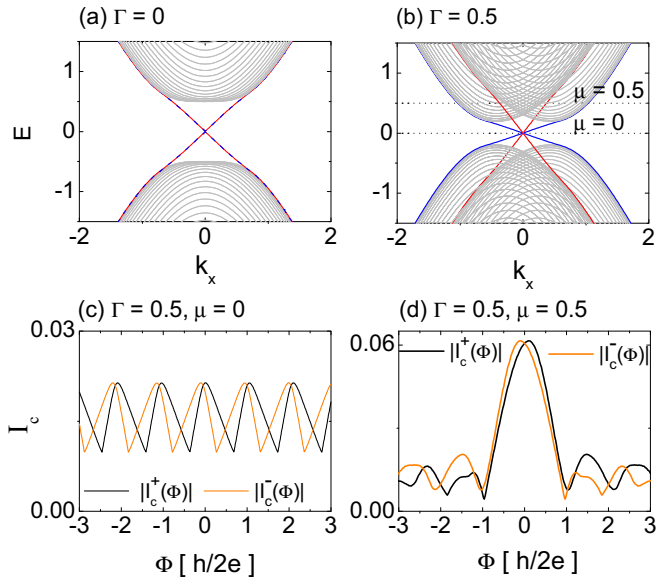

FIG. 2. (a), (b) Energy spectrums of a two-dimensional topological insulator with $\Gamma = 0$ and $\Gamma = 0.5$, respectively. When Γ is finite, the top (blue line) and bottom (red line) edges acquire different Fermi velocities v_{F1} and v_{F2}, respectively. In (c) and (d), superconductors are attached to the topological insulator to form a Josephson junction as shown in Fig. 1. The pairing potential is $\Delta = 0.05$. Panels (c) and (d) depict the critical current $I_c^{\pm}(\Phi)$ (in the unit of $eA/\hbar$) as a function of magnetic flux $\Phi[h/2e]$ of the Josephson junction for $\Gamma = 0.5$ at chemical potential $\mu = 0$ and $\mu = 0.5$ respectively. As shown in (b), at $\mu = 0$, only the edge states contribute to the transport. It is clearly shown in (c) that $|I_c^+(\Phi)| \neq |I_c^-(\Phi)|$ and $|I_c^+(\Phi)| \neq |I_c^+(-\Phi)|$. (d) At $\mu = 0.5$, the bulk states also contribute to the bulk transport. AJE is more pronounced when edge states dominate the transport. The model parameters are $A = 1$, $m_1 = 1$, and $m_0 = -0.5$.

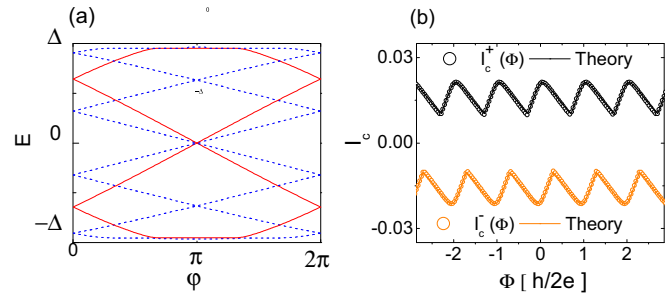

FIG. 3. (a) Andreev bound state spectrum of the superconductor/2D topological insulator/superconductor junction as a function of φ when inversion symmetry is broken with $\Gamma = 0.5$. The dashed solid blue lines and red lines denote the energy spectrum of upper and lower edges, respectively. The superconducting paring potential $\Delta = 0.05$ and other parameters are the same as those of Fig. 2(b). (b) The numerical results of Fig. 2(c), which shows the AJE, can be easily reproduced using the phenomenological theory using different I_{1n} and I_{2n} in the presence of magnetic field [29].

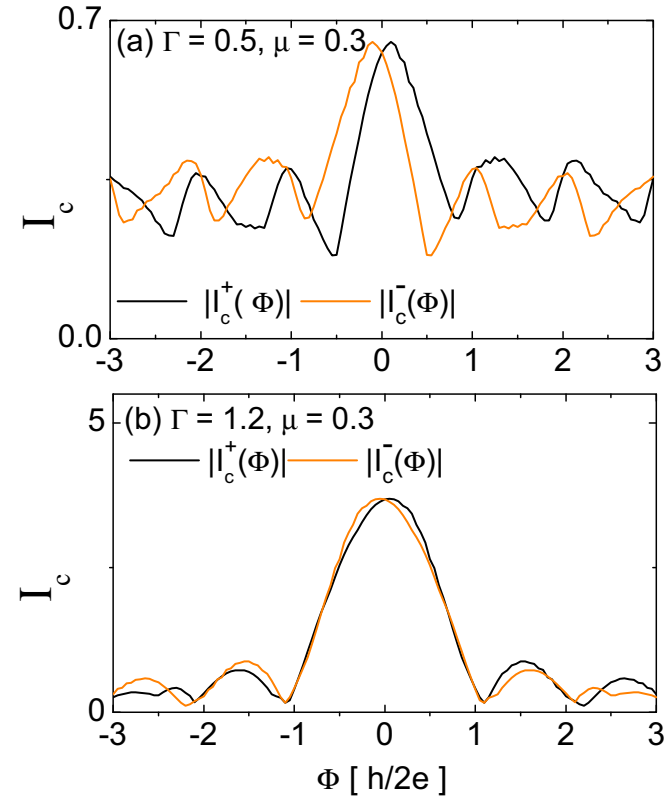

FIG. 4. Panels (a) and (b) show critical Josephson current $I_c^{\pm}$ (in the unit of $eA/\hbar$) vs magnetic flux $\Phi[h/2e]$ for type-I Weyl semimetal $\Gamma = 0.5$ and type-II Weyl semimetal $\Gamma = 1.2$, respectively. The Josephson current is mediated by both the Fermi arcs on the surface and the Weyl nodes in the bulk, because of $I_c^{\pm}$ has a central peak. AJE is more pronounced when the Fermi arc surface states dominate the transport. The parameters are $\Delta = 0.05$, $m_0 = -0.2$, and $t_z = 1.5$.

in the y direction and there are helical edge states propagating at the edge of the sample. The top edges (blue lines) and bottom edges (red lines) have the same Fermi velocity in the presence of the inversion symmetry [Fig. 2(a)], while the Fermi velocities are different if the inversion symmetry is broken with $\Gamma = 0.5$ [Fig. 2(b)]. This topological insulator can form a Josephson junction with two superconductors as shown in Fig. 1, where $\Delta e^{\pm i\varphi/2}$ denotes the pairing order parameter of the superconductors. Figures 2(c) and 2(d) depict the critical Josephson current as a function of magnetic flux Φ at the temperature $T = \Delta/30$ by recursive Green's function [26,27]. Here, we assume that fermion parity is not conserved at the junction so that the 4π Josephson effect is absent and this is consistent with the results of a recent experiment [28].

In the presence of inversion symmetry, the critical Josephson currents are the same in opposite directions, namely, $|I_c^+(\Phi)| = |I_c^-(\Phi)|$. Surprisingly, when inversion symmetry is broken as shown in Figs. 2(c) and 2(d), the critical current across the junction I_c^+ does not equal to the critical current flowing in the opposite direction I_c^- at fixed magnetic field such that $|I_c^+(\Phi)| \neq |I_c^-(\Phi)|$. Moreover, the critical currents also manifests asymmetric Fraunhofer patterns as depicted in Figs. 2(c) and 2(d) such that $|I_c^{\pm}(\Phi)| \neq |I_c^{\pm}(-\Phi)|$. This is in sharp contrast to conventional Josephson effect and we call this phenomenon the asymmetric Josephson effect. It is important to note that the directional dependence of the critical current $|I_c^+(\Phi)| \neq |I_c^-(\Phi)|$ and the asymmetric Fraunhofer pattern are connected to each other. Due to the time-reversal invariant, we have the condition that the critical current is unchanged when both the direction of the current and the direction of the magnetic field are changed, namely, $|I_c^+(\Phi)| = |I_c^-(-\Phi)|$. As a result, $|I_c^+(\Phi)| \neq |I_c^-(\Phi)|$ implies $|I_c^{\pm}(\Phi)| \neq |I_c^{\pm}(-\Phi)|$. It is important to note that asymmetric Fraunhofer pattern similar to Fig. 2(d) has been observed recently [28], but the origin of the effect was not known. In this work, we provide an explanation of the asymmetric Fraunhofer pattern.

To understand the origin of the AJE, we investigate the energy spectrum of Andreev bound states in the Josephson junction. In the presence of inversion symmetry, the energy spectrum has twofold degeneracies, since the top edges and bottom edges have exactly the same spectrum. On the other hand, the energy spectrum of Andreev bound states from the top edges and bottom edges are different in Fig. 3(a), because the two edge states have different Fermi velocities when the inversion symmetry is broken. As a result, the supercurrent from the top edges I_1 and the bottom edges I_2 are different due to the different Andreev bound-state spectrums of the two edges. This gives rise to AJE as discussed below.

III. PHENOMENOLOGICAL THEORY

In general, the total Josephson current $I(\Phi, \varphi)$ carried by the two edges states can be described as [27]

$$I(\Phi, \varphi) = \sum_{n=1}^{m} I_{1n} \sin(n\varphi + n\Phi) + I_{2n} \sin(n\varphi - n\Phi).$$

Here, I_{ln} indicates the Josephson current carried by the l edge at nth order, Φ represents the magnetic phase in the normal region, and φ is the phase difference between two s-wave superconductors. If the top edge current I_1 is the same as the bottom edge current I_2 due to inversion symmetry, we have $I_{1n} = I_{2n}$ and the Josephson current can be written as $I(\Phi, \varphi) = \sum_{n=1}^{m} (I_{1n} + I_{2n}) \cos(n\Phi) \sin(n\varphi)$. This implies that the Josephson current is always symmetric with respect to the signs of the magnetic field, namely, $I(\Phi, \varphi) = I(-\Phi, \varphi)$. In general, the top and bottom edges can have different energy spectrums due to inversion symmetry breaking as discussed above. Therefore, the two sets of coefficients I_{1n} and I_{2n} can be different.

In Fig. 3(b), we show that the numerical results of the Josephson current $I_c^{\pm}$ as a function of flux Φ can be well fitted to phenomenological theory (solid lines). The asymmetric critical Josephson currents are fitted by the $I_{1n} \neq I_{2n}$ and the Josephson currents of two edge states have the different magnitudes, which results from the asymmetric Fermi velocity of the two edge states $v_{F1} \neq v_{F2}$ as we discussed above. The consistency between the phenomenological theory and numerical results demonstrates that the AJE originates from the different Fermi velocities of the two sets of edge modes.

IV. AJE IN WEYL SEMIMETALS

Next we show that the Fermi arc states of Weyl semimetal can give rise to pronounced AJE in the a superconductor/Weyl semimetal/superconductor junction. Stacking the two-dimensional TI Hamiltonian H_{TI} in the z direction, we obtain a three-dimensional Weyl semimetal Hamiltonian [30,31],

$$\mathcal{H} = \sum_{\mathbf{k}} \psi_{\mathbf{k}}^{\dagger} \{\Gamma \sin k_x \tau_0 \sigma_3 + (M_{\mathbf{k}} - t_z \cos k_z)\tau_3 \sigma_0 + A \sin k_x \tau_1 \sigma_3 + A \sin k_y \tau_2 \sigma_0\} \psi_{\mathbf{k}}, \quad (2)$$

where the Pauli matrices $\tau_{1,2,3}$ (σ_3) and the unit matrix $\tau_0(\sigma_0)$ are defined in the orbital (spin) space, and $\psi_{\mathbf{k}}^{\dagger}$ is a four-component fermionic operator with momentum $\mathbf{k}$. $t_z = 1.5$ is the hopping energy in the z direction and A couples two orbitals in the x-y plane. Here $M_{\mathbf{k}} = m_0 + 2m_1(2 - \cos k_x - \cos k_y)$ determines the position of Weyl nodes with $m_0 = -0.2$. The Weyl nodes are located at $[0,0,\pm \arccos(m_0/t_z)]$, while the inversion symmetry breaking Γ term creates a tilted effect to the Weyl nodes [31]. The Weyl nodes are type I for $\Gamma < A$ and become type II when $\Gamma > A$ [31–33]. In general, the projections of the Weyl points on the surface Brillouin zones are connected by Fermi arcs, which result in conducting surface states on the surface of the Weyl semimetal. These surface arc states on two opposite surfaces of the Weyl semimetal can have different Fermi velocities when inversion symmetry is broken by Γ. This will give rise to the AJE in the superconductor/Weyl semimetal/superconductor junction in the following.

In Fig. 4, the Josephson current is mediated by both the Fermi arc states on the surface as well as the states near the Weyl nodes in the bulk. In this case, we can find pronounced AJE for type-I Weyl semimetal in Fig. 4(a), namely, the critical current across the junction I_c^+ does not equal to the critical current flowing in the opposite direction I_c^- at fixed magnetic field such that $|I_c^+(\Phi)| \neq |I_c^-(\Phi)|$. Moreover, the AJE is also

manifested by the asymmetric Fraunhofer pattern in which $|I_c^{\pm}(\Phi)| \neq |I_c^{\pm}(-\Phi)|$ as shown in Fig. 4(a). In Fig. 4(b), the AJE is also observed for type-II Weyl semimetal, even though there are more Josephson currents carried by the bulk states in type-II Weyl semimetals. Therefore, we conclude that AJE is more pronounced for surface-state dominated transport and it can be used as a transport signature for broken inversion symmetry (or surface and edge states with differing Fermi velocities) in topological insulators and Weyl semimetals.

V. DISCUSSION AND CONCLUSION

In summary, we uncovered an unusual Josephson effect in the inversion symmetry breaking topological materials. It is found that the magnitude of critical Josephson current across the junction I_c^+ does not equal the critical Josephson current flowing in the opposite direction I_c^- at fixed magnetic field B such that $|I_c^+(B)| \neq |I_c^-(B)|$. We call this phenomenon AJE. This can give rise to asymmetric Fraunhofer patterns which violate $|I_c^{\pm}(B)| = |I_c^{\pm}(-B)|$. This is in sharp contrast to conventional Josephson junctions. The AJE is a very general phenomenon, which can originate from topologically nontrivial or trivial surface states with differing Fermi velocities. We emphasize that the AJE discussed here is an intrinsic property of the system, which is distinct from the asymmetric Fraunhofer patterns induced by an external in-plane magnetic field with in-plane component [34]. Interestingly, the AJE shown in Fig. 2(d) qualitatively agrees with recently observed asymmetric Fraunhofer pattern in superconductor/quantum spin Hall insulator/superconductor Josephson junction [28]. They found that the critical current violates $|I_c^+(B)| = |I_c^-(B)|$ but follows the symmetry relation $|I_c^+(B)| = |I_c^-(-B)|$, which is the same as what we discussed here.

ACKNOWLEDGMENTS

We thank P. A. Lee, B. T. Zhou, and D.-H. Xu for illuminating discussions. The authors acknowledge the support of HKRGC and Croucher Foundation through Grants No. HKUST3/CRF/13G, No. 602813, No. 605512, and No. 16303014 and a Croucher Innovation grant. K.C.F. thanks Raytheon BBN Technologies for funding support. M.N.A. acknowledges the support of the Alexander von Humboldt Foundation's Sofia Kovalevskaja Award and G.-H.L. was supported by the National Research Foundation of Korea (NRF) Grant funded by the Korean Government (No. 2016R1A5A1008184).

[1] M. Z. Hasan and C. L. Kane, Rev. Mod. Phys. **82**, 3045 (2010).
[2] X.-L. Qi and S.-C. Zhang, Rev. Mod. Phys. **83**, 1057 (2011).
[3] X. Wan, A. M. Turner, A. Vishwanath, and S. Y. Savrasov, Phys. Rev. B **83**, 205101 (2011).
[4] A. A. Burkov and L. Balents, Phys. Rev. Lett. **107**, 127205 (2011).
[5] H. Weng, C. Fang, Z. Fang, B. A. Bernevig, and X. Dai, Phys. Rev. X **5**, 011029 (2015).
[6] S. M. Huang, S. Y. Xu, I. Belopolski, C. C. Lee, G. Q. Chang, B. K. Wang, N. Alidoust, G. Bian, M. Neupane, A. Bansil, H. Lin, and M. Z. Hasan, Nat. Commun. **6**, 7373 (2015).
[7] S. Y. Xu, C. Liu, S. K. Kushwaha, R. Sankar, J. W. Krizan, I. Belopolski, M. Neupane, G. Bian, N. Alidoust, T. R. Chang, H. T. Jeng, C. Y. Huang, W. F. Tsai, H. Lin, P. P. Shibayev, F. C. Chou, R. J. Cava, and M. Z. Hasan, Science **347**, 294 (2015).
[8] B. Q. Lv, H. M. Weng, B. B. Fu, X. P. Wang, H. Miao, J. Ma, P. Richard, X. C. Huang, L. X. Zhao, G. F. Chen, Z. Fang, X. Dai, T. Qian, and H. Ding, Phys. Rev. X **5**, 031013 (2015).
[9] L. Huang, T. M. McCormick, M. Ochi, Z. Zhao, M.-T. Suzuki, R. Arita, Yun Wu, D. Mou, H. Cao, J. Yan, N. Trivedi, and A. Kaminski, Nat. Mater. **15**, 1155 (2016).
[10] K. Deng, G. Wan, P. Deng, K. Zhang, S. Ding, E. Wang, M. Yan, H. Huang, H. Zhang, Z. Xu, J. Denlinger, A. Fedorov, H. Yang, W. Duan, H. Yao, Y. Wu, S. Fan, H. Zhang, X. Chen, and S. Zhou, Nat. Phys. **12**, 1105 (2016).
[11] H. Nielsen and M. Ninomiya, Phys. Lett. B **130**, 389 (1981).
[12] D. T. Son and B. Z. Spivak, Phys. Rev. B **88**, 104412 (2013).
[13] H.-J. Kim, K.-S. Kim, J.-F. Wang, M. Sasaki, N. Satoh, A. Ohnishi, M. Kitaura, M. Yang, and L. Li, Phys. Rev. Lett. **111**, 246603 (2013).
[14] J. Xiong, S. K. Kushwaha, T. Liang, J. W. Krizan, M. Hirschberger, W. Wang, R. J. Cava, and N. P. Ong, Science **350**, 413 (2015).
[15] X. Huang, L. Zhao, Y. Long, P. Wang, D. Chen *et al.*, Phys. Rev. X **5**, 031023 (2015).
[16] C. Z. Li, L. X. Wang, H. W. Liu, J. Wang, Z. M. Liao, and D. P. Yu, Nat. Commun. **6**, 10137 (2015).
[17] A. Lucas, R. A. Davison and and S. Sachdev, Proc. Natl. Acad. Sci. USA **113**, 9463 (2016).
[18] M. Hirschberger, S. Kushwaha, Z. Wang, Q. Gibson, C. A. Belvin, B. A. Bernevig, R. J. Cava, and N. P. Ong, Nat. Mater. **15**, 1161 (2016).
[19] J. Gooth *et al.*, Nature (London) **547**, 324 (2017).
[20] A. C. Potter, I. Kimchi, and A. Vishwanath, Nat. Commun. **5**, 5161 (2014).
[21] P. J. Moll, N. L. Nair, T. Helm, A. C. Potter, I. Kimchi, A. Vishwanath, and J. G. Analytis, Nature (London) **535**, 266 (2016).
[22] A. Chen, D. I. Pikulin, and M. Franz, Phys. Rev. B **95**, 174505 (2017).
[23] O. O. Shvetsov, A. Kononov, A. V. Timonina, N. N. Kolesnikov, and E. V. Deviatov, JETP Letters (2018), doi:10.1134/S0021364018120020.
[24] D. G. Rothe, R. W. Reinthaler, C.-X. Liu, L. W. Molenkamp, S.-C. Zhang, and E. M. Hankiewicz, New J. Phys. **12**, 065012 (2010).
[25] B. A. Bernevig, T. L. Hughes, and S.-C. Zhang, Science **314**, 1757 (2006).
[26] A. Furusaki, Physica B (Amsterdam) **203**, 214 (1994); Y. Asano, Phys. Rev. B **63**, 052512 (2001).
[27] Y. Asano, Y. Tanaka, M. Sigrist, and S. Kashiwaya, Phys. Rev. B **67**, 184505 (2003).

[28] E. Bocquillon, R. S. Deacon, J. Wiedenmann, P. Leubner, T. M. Klapwijk, C. Brüne, K. Ishibashi, H. Buhmann, and L. W. Molenkamp, Nat. Nanotechnol. **12**, 137 (2017).

[29] In the fitting of Fig. 3, the magnetic flux is redefine as $\Phi = A_{\text{eff}} \times B$ to include the finite broadening of the edge states, where B is the magnetic field and $A_{\text{eff}} = L \times W/1.05$ is the effective area with the length L and the width W.

[30] S. Kourtis, J. Li, Z. Wang, A. Yazdani, and B. A. Bernevig, Phys. Rev. B **93**, 041109 (2016).

[31] M. J. Park, B. Basa, and M. J. Gilbert, Phys. Rev. B **95**, 094201 (2017).

[32] A. A. Soluyanov, D. Gresch, Z. Wang, Q. Wu, M. Troyer, X. Dai, and B. A. Bernevig, Nature (London) **527**, 495 (2015).

[33] Y. Xu, F. Zhang, and C. Zhang, Phys. Rev. Lett. **115**, 265304 (2015).

[34] H. J. Suominen, J. Danon, M. Kjaergaard, K. Flensberg, J. Shabani, C. J. Palmstrøm, F. Nichele, and C. M. Marcus, Phys. Rev. B **95**, 035307 (2017).